Aeroacoustics Conferences
20-23 May 2019, Delft, The Netherlands
25th AIAA/CEAS Aeroacoustics Conference

10.2514/6.2019-2473

Modelling Noise from Offset Two-Stream Jets Using Linear Stability Theory and Kirchhoff Surface Method

Nitya Singh[*], Nikhil Sohoni[†] and Aniruddha Sinha[‡]
Dept. of Aerospace Engineering, Indian Institute of Technology Bombay, Mumbai 400076, INDIA

Dual-stream high-bypass ratio jet engines are ubiquitous in civilian aviation for their efficiency and quiet operation. One of the recent concepts for further reducing their radiated noise preferentially towards the ground, is to offset the horizontal secondary stream downward with respect to the primary stream. To understand the consequent noise benefit and design further improvements, we deploy linear stability theory as a model for the noise sources, as has been done often in the recent past for simpler jet configurations. The instability wave packets derived therefrom do indeed display a preferential weakening in the bottom sector of the jet. Mach wave radiation occurs from the primary jet as it is convectively supersonic; this is modelled by applying the Kirchhoff surface method to the wave packets. The far acoustic field thus obtained also displays the beneficial azimuthal distortion. The theory proposed here thus provides a tool to study and refine sophisticated jet noise reduction concepts.

I. Introduction

The bypass stream of modern turbofan jet engines not only provides benefits in cycle efficiency but also mitigate jet exhaust noise significantly. The latter may be understood in terms of a reduction in average exhaust velocity and temperature with increasing bypass ratio, keeping the thrust constant. The radiated noise scales as a high power of the jet velocity – eighth power at low subsonic speeds (as famously calculated by Lighthill [1]) and with smaller exponents at higher speeds. On the other hand, the scaling with jet exit area is linear. The net effect is a reduction in radiated noise with increasing bypass. Leveraging this powerful principle, engineers have increased bypass ratios to 10:1 or more, resulting in substantial quietening. However, further improvements in this direction are difficult owing to mechanical issues related to large moving parts at high bypass ratios.

Another way of understanding the noise reduction is in terms of shielding of the noise sources in the primary shear layer (between the core and bypass streams) by the slower secondary potential core and shear layer (between the bypass stream and the ambient) [2,3]. This perspective is more useful for analyzing the azimuthal variations in radiated noise from non-axisymmetric nozzle arrangements – the focus of this study.

Indeed, some recent research efforts have been concerned with finding ways of preferentially quietening the bottom azimuthal sector of the jet to mitigate noise radiation to ground personnel as well as communities. This is typically obtained at the expense of increasing noise levels at other azimuthal sectors, especially at the top, while maintaining the overall thrust from the jet constant. The ideas proposed for achieving this include offsetting the secondary jet downwards relative to the primary one [4], tilting downwards the secondary jet axis [2], and installing guide vanes in the secondary stream that direct it preferentially downwards [5]. The beneficial redistribution of the far-field noise in the above designs have been demonstrated in experiments. Tools have also been developed for predicting the noise modifications from RANS simulations of the Reynolds stress changes in the redesigned jets relative to the corresponding baseline coaxial jet [3].

We model the noise sources as linear Kelvin-Helmholtz (K-H) instability wave packets associated with the mean flow field. Such wave packets have been established as a useful model of the time-averaged growth of natural large-scale coherent structures in a turbulent shear layer [6,7]. These low-frequency low-azimuthal

[*]M.Tech. Student
[†]Ph.D. Student
[‡]Assosciate Professor; AIAA Member; Corresponding author: as@aero.iitb.ac.in

complexity coherent structures are, in turn, associated with the noise radiated to the loudest aft sector of high-speed turbulent jets[8]. The theory is applied to limited mean flow data of a Mach 1.5 – Mach 0.9 two-stream jet reported by Murakami and Papamoschou[4].

In this paper, we extend and expand upon our earlier work along these lines, as presented by Sohoni and Sinha[9]. The main points of distinction of the present work are the following: (a) a more accurate parameterization of the mean flow field from available offset jet data, (b) expansion of the study to wave packets at multiple Strouhal numbers, (c) extension of the calculations to far downstream stations, and (d) a preliminary attempt at prediction of the acoustic far-field of the wave packets. We further substantiate our earlier hypothesis that the parallel-flow linear stability analysis can indicate the trends in acoustic far-field modifications with variations in the degree of offset between the primary and secondary streams of the jet.

II. Linear stability theory and acoustic propagation for offset jets

A. Linear stability theory

The parallel flow linear stability theory is strictly applicable to laminar base flows. However, recent results from resolvent analysis[10,11] justify its extension to turbulent mean flows. In particular, the applicability is limited to a range of Strouhal numbers and azimuthal Fourier modes at which the least stable resolvent mode is well-separated from all other more stable resolvent modes. It is fortunate that this range happens to be relevant for the dominant far-field noise radiation owing to the significant coherence of these modes.

The base flow for offset jets, if assumed to be quasi parallel in the streamwise direction (x, say), still has two inhomogeneous directions ($y-z$ in Cartesian coordinates, or $r-\theta$ in cylindrical coordinates). Thus, the linear stability analysis gives rise to a bi-global eigenvalue problem, instead of being one-dimensional (in r) as in axisymmetric jets. To connect and compare results with axisymmetric jets, we prefer cylindrical coordinates (x, r, θ). Moreover, we perform the analysis in the azimuthal Fourier domain instead of in the θ–domain, the former approach being best suited for the reference axisymmetric jet. Results are presented in the $y-z$ domain though for ease of comprehension.

Let the relevant flow variable vector be denoted by $\boldsymbol{q} := [u, v, w, p, \zeta]^{\mathrm{T}}$, comprising the three cylindrical components of velocity, pressure and specific volume. Velocities are normalized by the ambient speed of sound a_∞, and lengths by the primary nozzle exit diameter D_p. The specific volume is normalized by its ambient value ζ_∞, and pressure by a_∞^2/ζ_∞. The locally-parallel mean flow vector is $\overline{\boldsymbol{q}}\,(r, \theta)$, and the fluctuations $\boldsymbol{q}'$ about $\overline{\boldsymbol{q}}$ are governed by the linearized compressible Navier-Stokes equations represented in matrix form as

$$\left\{\mathscr{L}^0 + \mathscr{L}^t \frac{\partial}{\partial t} + \mathscr{L}^x \frac{\partial}{\partial x} + \mathscr{L}^r \frac{\partial}{\partial r} + \mathscr{L}^\theta \frac{\partial}{\partial \theta} + \sum_{\zeta,\tau \in \{x,r,\theta\}} \mathscr{L}^{\zeta\tau} \frac{\partial^2}{\partial\zeta\partial\tau}\right\}\boldsymbol{q}' = \boldsymbol{0}. \quad (1)$$

Here, the 5×5 matrices $\mathscr{L}$ are functions of $\overline{\boldsymbol{q}}$ in general.

As is usual, we employ the following normal mode ansatz:

$$\boldsymbol{q}'(x, r, \theta, t) = \tilde{\boldsymbol{q}}(r, \theta)\mathrm{e}^{\iota(\alpha x - \omega t)} + \text{c.c.}, \qquad \tilde{\boldsymbol{q}}(r, \theta) = \sum_{m=-\infty}^{\infty} \hat{\boldsymbol{q}}_m(r)\mathrm{e}^{\iota m\theta}. \quad (2)$$

In the spatial stability analysis, the temporal frequency ω is real, whereas the axial wavenumber α is complex; $\tilde{\boldsymbol{q}}$ represents the shape function of the fluctuation in the polar plane. The real part of α (denoted α_r) is inversely proportional to the wavelength, whereas the negative of the imaginary part $(-\alpha_i)$ is the growth rate of the instability. We refer to a particular ω by the corresponding Strouhal number $St := \omega D_p/(2\pi U_p)$, where U_p is the primary nozzle exit velocity. In the azimuthal Fourier domain, m is the mode number, and $\hat{\boldsymbol{q}}_m$ is the mth azimuthal mode of the shape function. Substitution of this ansatz in eqn. (1) yields

$$\begin{aligned} -\iota\omega\hat{\mathscr{L}}^t\hat{\boldsymbol{q}}_m + \sum_{n=-N}^{N} \Bigg[\Bigg\{ \hat{\mathscr{L}}_n^0 + \hat{\mathscr{L}}_n^r \frac{\partial}{\partial r} + \hat{\mathscr{L}}_n^{rr} \frac{\partial^2}{\partial r^2} + \iota\,(m-n) \left(\hat{\mathscr{L}}_n^\theta + \hat{\mathscr{L}}_n^{r\theta} \frac{\partial}{\partial r} \right) - (m-n)^2\, \hat{\mathscr{L}}_n^{\theta\theta} \Bigg\} \\ + \iota\alpha \left\{ \hat{\mathscr{L}}_n^x + \hat{\mathscr{L}}_n^{xr} \frac{\partial}{\partial r} + \iota\,(m-n)\, \hat{\mathscr{L}}_n^{\theta x} \right\} - \alpha^2 \left\{ \hat{\mathscr{L}}_n^{xx} \right\} \Bigg] \hat{\boldsymbol{q}}_{m-n} = \boldsymbol{0}, \qquad m \in [-S, S]. \quad (3) \end{aligned}$$

Here, we assume that the Fourier azimuthal complexity of the mean flow (and hence that of the dependent operators) is limited to $[-N, N]$. Consequently, the complexity of the fluctuations is also assumed to be limited to $[-S, S]$, with $S \geq N$; this is analogous to the usual limit placed on azimuthal grid resolution. Thus we obtain a set of coupled equations that comprises a quadratic eigenvalue problem. This is to be contrasted with the case of an axisymmetric jet, wherein all the azimuthal Fourier modes are decoupled. The quadratic term is usually neglected by appealing to its relative unimportance, involving as it does the second-order x-derivative of the fluctuations.

Owing to the presumed uniformity of the flow at the centreline and far field, boundary conditions are formulated at the centreline using the pole treatment described by Mohseni and Colonius [12] and in the far field using the non-reflecting characteristic formulation of Thompson [13]. The radial domain is discretized with a grid clustered preferably in the shear layer, and fourth-order central differences are used to obtain a sparse matrix eigenvalue problem. It is solved with the ARPACK library [14] in a parallelized manner.

As the jet is spreading downstream, the quasi-parallel stability analysis is performed at several x–stations to obtain respective eigensolutions $\{\alpha(x), \tilde{\boldsymbol{q}}(r, \theta; x)\}$. Note that we have made the x–dependence of the eigenfunction solution explicit. To model the growth and saturation of the instability wave packets, the individual eigensolutions can be combined to obtain a composite eigenfunction [9,15] as follows:

$$\tilde{\boldsymbol{Q}}(x, r, \theta) = \sum_{m=-S}^{S} \hat{\boldsymbol{Q}}_m(x, r)\, \mathrm{e}^{\iota m\theta}, \qquad \hat{\boldsymbol{Q}}_m(x, r) := \hat{\boldsymbol{q}}_m(r; x)\, \mathrm{e}^{\iota \int_{x_0}^{x} \alpha(\xi)\mathrm{d}\xi}, \tag{4}$$

where x_0 is the first axial station at which the stability problem is solved. To ensure that the shape function $\tilde{\boldsymbol{q}}(r, \theta; x)$ varies slowly in x, the individual eigenfunctions at each x–station are separately normalized to have maximum magnitude of unity over the $r - \theta$ domain. Moreover, their phase is set to vanish at the point of maximum. This ensures that the wave-like behaviour of oscillation and growth/decay is captured predominantly by the exponential part, as hypothesized in the quasi-parallel flow analysis.

B. Acoustic propagation

Linear instability wave packets with supersonic phase speed couple directly with the acoustic far field through Mach wave radiation [8]. In such cases, the acoustic field prediction from these wave packets has been found to be validated quite well by large-eddy simulation data [16]. On the other hand, instability wave packets with subsonic phase speed are very inefficient radiators of sound, and other mechanisms like jitter [17] and nonlinearity [18] that are not modelled here assume greater significance. In these cases, the direct acoustic prediction from the wave packets is poor [17] and should not be pursued.

If the linear instability wave packets have supersonic phase speed, then a Kirchhoff surface approach [19] can be applied to obtain the sound field. The assumption is that at a short radial distance from the jet, say $r = r_{KS}$, the base flow is quiescent and the fluctuations are irrotational, so that the low-amplitude pressure fluctuations are essentially governed by the free-space three-dimensional linear wave equation. Anticipating the consequent decoupling of the solution in the axial and azimuthal Fourier domain, we define the axial and azimuthal Fourier transform of the composite pressure eigenfunction as

$$\check{P}_m(r; k) := \int_{x_0}^{x_f} \hat{P}_m(x, r)\, W(x) \mathrm{e}^{-\iota k x} \mathrm{d}x, \quad \hat{P}_m(x, r) = \frac{1}{2\pi} \int \check{P}_m(r; k) \mathrm{e}^{\iota k x} \mathrm{d}k. \tag{5}$$

Here, x_0 is the initial axial station of the calculation as before, x_f is the final station, k is the (real) axial wavenumber, and $W(x)$ is a window function to be described subsequently.

With this, the wave equation in cylindrical coordinates becomes the Helmholtz equation, with boundary condition specified on the Kirchhoff cylinder of radius r_{KS}. Then, retaining the outgoing waves only, the acoustic solution at any point outside the cylinder is given by

$$\check{P}_m(r; \omega, k) = \check{P}_m(r_{KS}; \omega, k) \frac{H_m^{(1)}(r\sqrt{\omega^2 - k^2})}{H_m^{(1)}(r_{KS}\sqrt{\omega^2 - k^2})}, \qquad r > r_{KS}, \quad \omega > 0, \quad |k| < \omega. \tag{6}$$

Here, $H_m^{(1)}$ is the mth order Hankel function of the first kind, the dependence of the solution on ω is made explicit, and the constraint on k comes from the radiation condition. Note that if ω were negative, then the Hankel function of the second kind would have been used. The pressure fluctuations propagated to the observer coordinate (x, r, θ) may be found by performing the appropriate inverse Fourier transforms in x and θ on the above solution.

The axial extent of the calculation domain is limited to the region where the K-H mode is unstable, as the linear stability analysis results are difficult to interpret once the modes become stable. This leads to truncation of the wave packet at its peak, prior to the decay zone. To reduce the errors associated with the direct use of this data in the acoustic calculation, the following window function $W(x)$ is used[19]

$$\breve{W}(x) := \frac{1}{2}\left[\tanh\left(5\frac{x-x_1}{x_1-x_0}\right) - \tanh\left(5\frac{x_2-x}{x_f-x_2}\right)\right], \quad W(x) = \breve{W}(x)\left(\frac{1}{x_f-x_0}\int_{x_0}^{x_f}\breve{W}^2(x)\mathrm{d}x\right)^{-1/2}. \quad (7)$$

Here, x_1 and x_2 are respectively the 5% and 95% points in the x–domain between x_0 and x_f. Such a window function is preferred over the more common Hanning function that is better suited to longer data series.

III. Mean flow field model

The sole input to our noise source model is the mean flow field of the offset dual-stream jet. In this paper, we will study the linear stability consequences of the degree of offset between the two streams. Furthermore, the analysis will be performed independently at several axial stations to track the spatial evolution of the K-H wave packet. Thus, we require a valid mean flow model that can accommodate this range of parameters. To the authors' knowledge, the only database of offset dual-stream jet mean flow field is reported by Murakami and Papamoschou[4]. This data provides guidance and validation for our mean flow model.

The mean axial velocity field was proposed earlier by us[9] as an extension of the truncated Gaussian function used commonly for jets[20]:

$$\begin{aligned}
&\overline{u}(x,y,z) = u_c(x)\left\{(1-h(x))\overline{u}_1(x,y,z) + h(x)\overline{u}_2(x,y,z)\right\},\\
&\overline{u}_k(x,y,z) = \begin{cases} 1, & \text{if } \sigma_k(y,z) < R_k(x),\\ \exp\left(-\dfrac{(\sigma_k(y,z)-R_k(x))^2}{\delta_k^2(x)}\right), & \text{otherwise,}\end{cases} \qquad k \in \{1,2\},\\
&\sigma_1(y,z) := \sqrt{y^2+z^2}, \qquad \sigma_2(y,z) := \sqrt{y^2+(z+C)^2}.
\end{aligned} \quad (8)$$

Here, the parameters R_1, R_2, δ_1, δ_2, h and u_c are found at various x–stations by fitting concentric jet data. Of the two truncated Gaussian functions $\overline{u}_1$ and $\overline{u}_2$, the first is concentric with the axis of the coordinate system, and the parameter C allows us to introduce a consistent offset of the second at all axial stations, presumably corresponding to a like offset between the two nozzles. Note that a positive value of C simulates the downward offset (along the negative z–axis) of the secondary stream relative to the primary stream.

To fit the above functions, we used the 'C17M90' coaxial and 'E17M90' eccentric jets[4]. The ratio of the secondary to primary nozzle exit diameters in both jets was 1.7; both jets had primary Mach number of 1.5 and secondary Mach number of 0.9. The eccentric jet was fully offset such that the two nozzles were touching at their top dead centers; this is equivalent to an offset of $C = 0.35$ in our notation. The mean axial velocity profiles at four axial stations in the two jets are excerpted from Murakami and Papamoschou[4] in fig. 1a. The coaxial jet function (setting $C = 0$ in eqn. (8)) is fitted to the 'C17M90' data, and appears to agree very well with the same. Figure 1b demonstrates that the fitting parameters vary smoothly with x. Note that these fits have been improved relative to our previous work[9].

Next, the fitting function is evaluated with the offset $C = 0.35$ keeping all other parameters the same, and the resulting mean velocity profiles are compared with the 'E17M90' data in fig. 1a. Clearly, the agreement is very good near the nozzle (implying that the two streams are evolving almost independent of each other), although significant discrepancies are evident further downstream. In particular, the potential core is apparent in the bottom sector of the eccentric jet even up to $x = 9$, whereas the fitted model fails to replicate this.

Figure 1c provides examples of the mean axial velocity field obtained from the fits. Note that we consistently follow the convention of displaying plots in this paper such that the applied offset thickens the secondary potential core at the bottom sector, as shown in these figures.

IV. Results

The linear stability of dual-stream coaxial round jets has been studied by several researchers[21–24]. The single-stream round jet is known to have at most one unstable eigensolution (viz. the K-H) mode for every

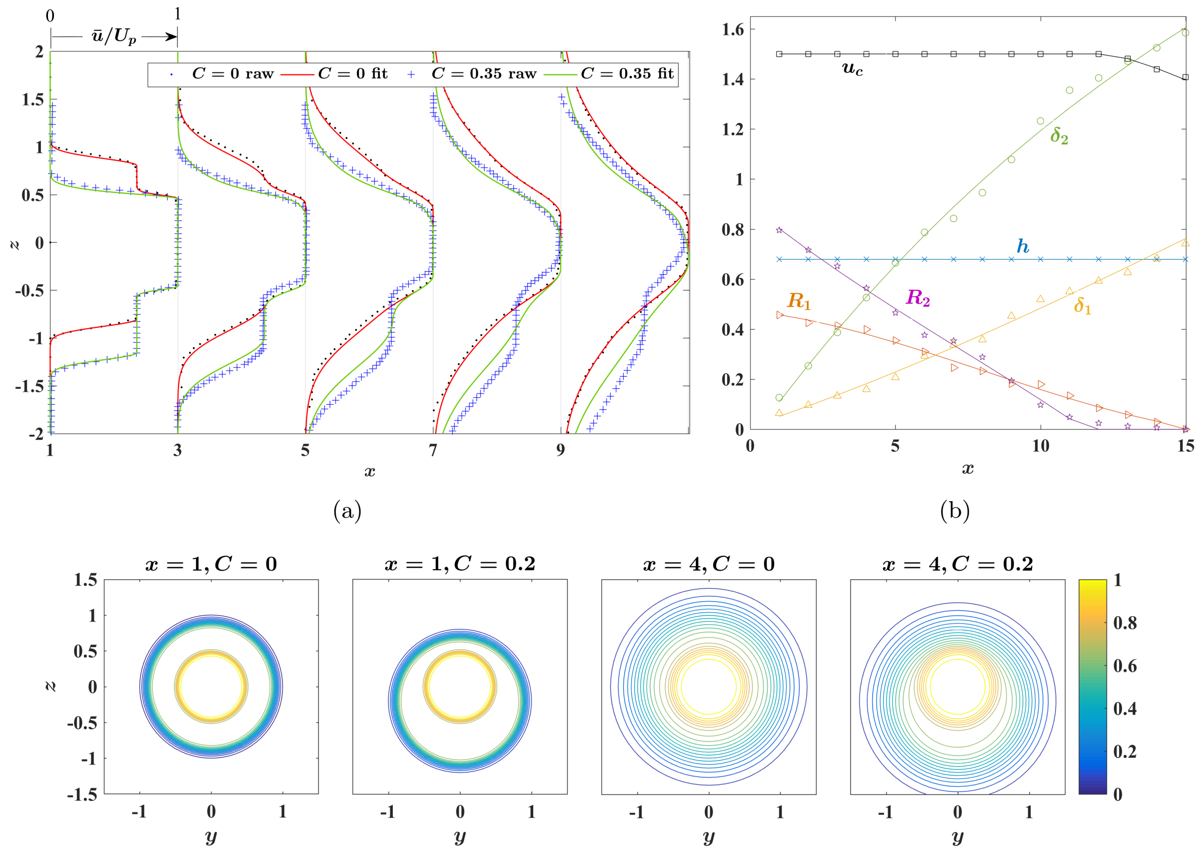

(a) (b) (c)

Figure 1: (a) Mean axial velocity profiles of C17M90 and E17M90 jets from Ref. 4 fitted with the function in eqn. (8). (b) The parameters of the fitting function, smoothed by cubic splines. (c) Example contour plots of $\overline{u}/U_p$ at two axial stations and with two offsets.

$St - m$ pair. Dual-stream round jets, on the other hand, generally have two K-H modes for every such pair – these are the inner and outer modes associated with the respective shear layers of the jet. The pressure component of the inner and outer eigenfunctions for the coaxial jet at $x = 1$ for $St = 0.1$ and 0.3 are portrayed in the first columns of each subfigure of fig. 2. Results are shown for the axisymmetric mode ($m = 0$), the first helical mode ($m = 1$) and the second helical mode ($m = 2$) in the three rows of each subfigure. Since the eigensolutions are symmetric about the $y = 0$ plane, only their right halves are shown. The parameters of the calculations are detailed in Appendix A.

As the offset is increased slightly from zero to $C = 0.05$ (see the second columns of each subfigure in fig. 2), the eigensolution becomes coupled in the m–domain; however, their azimuthal nature remains preserved approximately. Thus, although the bi-global stability solutions do not have a unique azimuthal Fourier mode m, they can be labelled based on their similarity with one of the coaxial jet modes. This label is the μ number of the eigensolution, which degenerates to the m number in the coaxial jet.

Although, the μ labelling is trivial at small offsets, it becomes complicated at larger offsets, as evidenced by fig. 2. To enable unambiguous tracking of eigensolutions with increasing C, we define the 'closeness' $\mathscr{C}_{1,2}$ of two pressure eigenfunctions $\tilde{p}_1(r, \theta)$ and $\tilde{p}_2(r, \theta)$ as

$$\mathscr{C}_{1,2} := \frac{|\langle \tilde{p}_1 \ , \ \tilde{p}_2 \rangle|}{||\tilde{p}_1|| \, ||\tilde{p}_2||}, \qquad \langle \tilde{p}_1 \ , \ \tilde{p}_2 \rangle := \int_{-\pi}^{\pi} \int_0^{\infty} \tilde{p}_2^{\dagger}(r, \theta) \tilde{p}_1(r, \theta) r \mathrm{d}r \mathrm{d}\theta, \qquad ||\tilde{p}|| := \sqrt{\langle \tilde{p} \ , \ \tilde{p} \rangle}. \tag{9}$$

Here, $(\cdot)^{\dagger}$ denotes the complex conjugate. To track a particular μ mode across variations of C (or, for that matter, any parameter like x, St), we choose the one eigenfunction at the current value of C that is 'closest' to the corresponding μ eigenfunction at the previous value of C (indicated by a value of $\mathscr{C}$ closest to unity).

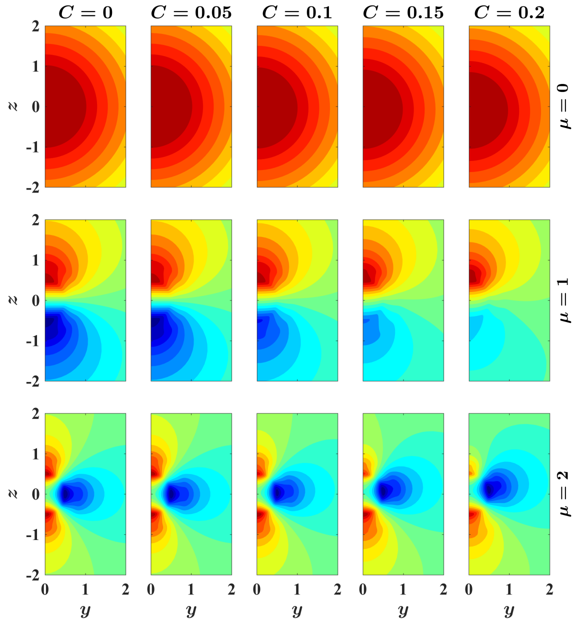

(a) Inner modes, $St = 0.1$.

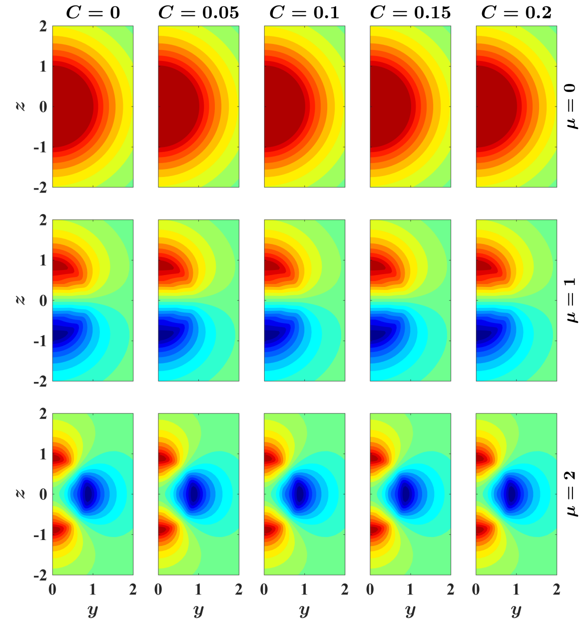

(b) Outer modes, $St = 0.1$.

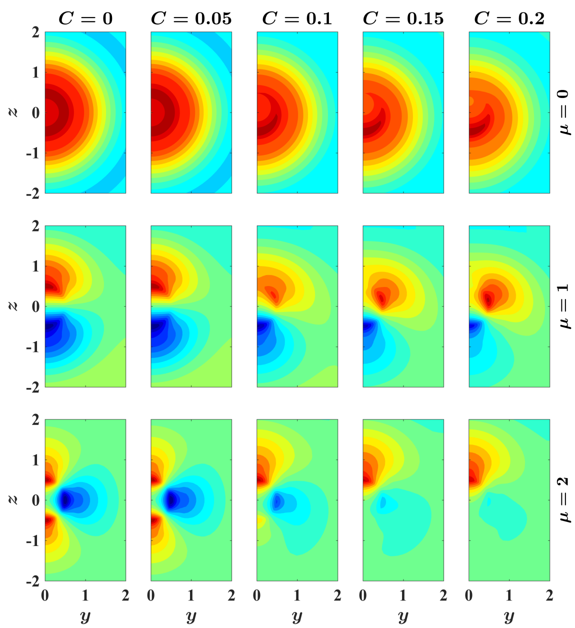

(c) Inner modes, $St = 0.3$.

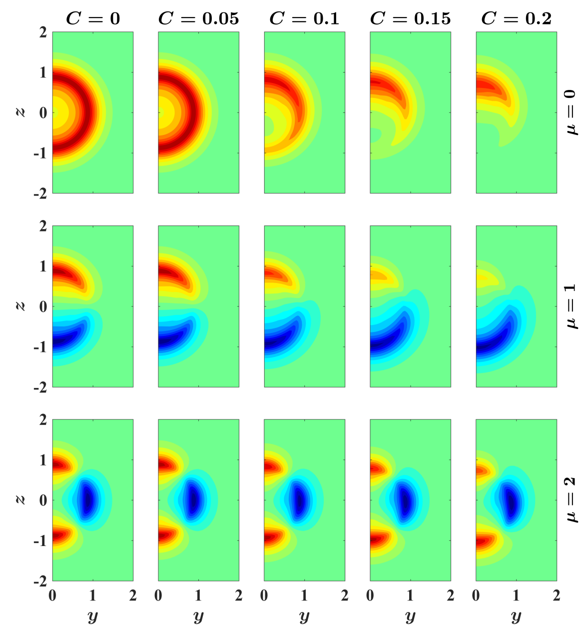

(d) Outer modes, $St = 0.3$.

Figure 2: Real parts of pressure eigenfunctions at $x = 1$ for (a, b) $St = 0.1$ and (c, d) $St = 0.3$, in both (a, c) inner and (b, d) outer modes. In each case, results are presented column-wise with various offsets C between the two streams of the jet, and row-wise for the first three μ modes. The orientation of the eigenfunction plots is such that the lower halves correspond to the thicker shear layer. Plots are symmetric about $y = 0$. Colour levels range from $+1$ (red) to -1 (blue).

The performance of this mode-tracking algorithm has already been evidenced by the similarity of the eigenfunctions labelled by a common μ in fig. 2. In fact, these figures allow us to comment on the modification of the instability eigenfunctions with increasing offset. The changes are generally small for $St = 0.1$, although some distortion is apparent in the inner modes for $\mu = 1$ and 2. The changes are much more pronounced

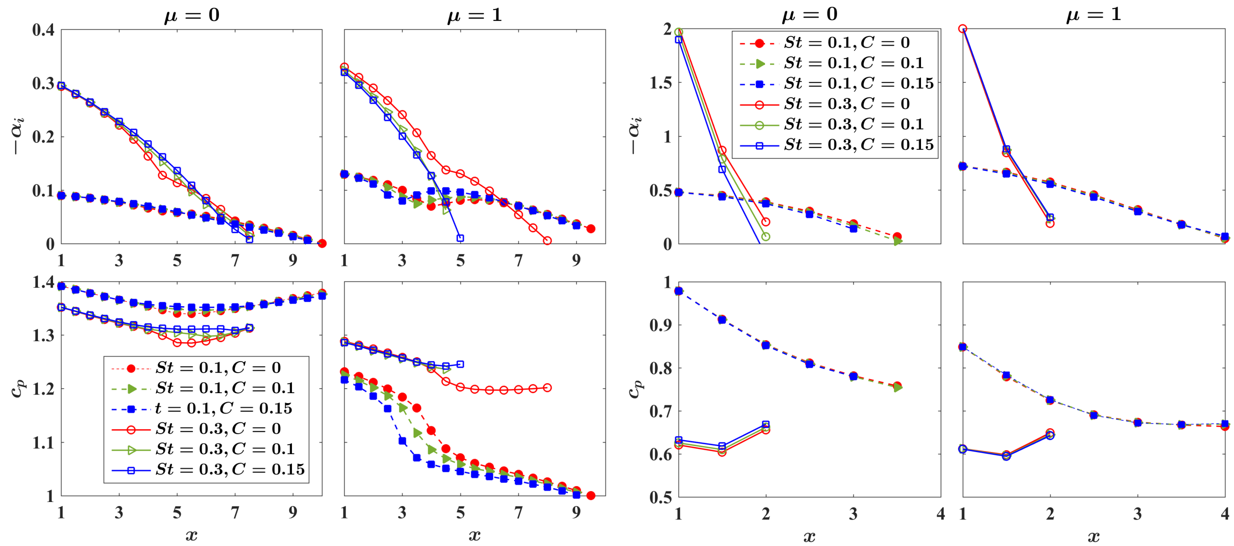

(a) Inner modes

(b) Outer modes

Figure 3: (a) Inner and (b) outer modes' eigenvalues (in terms of growth rate $-\alpha_i$ and phase speed c_p) vs. axial station for two μ cases (0 and 1), two frequencies ($St = 0.1$ and 0.3), and three offsets ($C = 0$, 0.1 and 0.15).

for $St = 0.3$. In the case of the inner modes, the $\mu = 0$ mode weakens in the top sector of the jet, whereas the $\mu = 1$ and 2 weaken in the bottom sector. The outer modes appear to have the opposite behaviour. Such preferential weakening is expected to modify the azimuthal homogeneity of the far acoustic field that is otherwise expected in an axisymmetric jet.

Here onwards, we focus on the $\mu = 0$ and 1 modes only. This is motivated by two observations: (a) the trends observed with $\mu = 2$ mode are similar to those for $\mu = 1$, and (b) the $\mu = 2$ mode is a less efficient radiator of sound than the $\mu = 1$ mode (and especially the $\mu = 0$ mode)[25], making it less relevant for noise studies.

Figure 3 presents the modifications of the various K-H modes' eigenvalues with increasing axial station and offset. The stability calculations were discontinued once the modes stabilize, as unambiguous tracking was not possible thereafter. The inner modes have supersonic phase speeds, owing to the Mach 1.5 primary jet; the outer modes have subsonic phase speeds. The disparity in phase speeds with frequency is stark for the outer modes. Compared to the $St = 0.1$ case, the $St = 0.3$ instability generally starts out with higher growth rate close to the nozzle, but stabilizes earlier. The outer modes stabilize much closer to the nozzle exit than the inner modes. This is explained by noting in fig. 1b that the outer shear layer's thickness parameter (δ_2) is consistently larger than that of the inner shear layer (δ_1). In general, the effect of offset is not very pronounced in the eigenspectra. However, earlier stabilization is observed in the $St = 0.1$, $\mu = 1$ inner mode.

We now move on to a discussion of the composite eigenfunctions, to investigate the wave packet nature of these instabilities, and connect them to the acoustic far field. The inner modes, owing to their supersonic phase speed, are expected to be very efficient radiators of sound. Thus, their modification with increasing offset of the dual-stream jet is of particular interest. Unfortunately, the linear stability analysis does not yield the absolute amplitudes of the wave packets; they can only provide the shapes up to an arbitrary scalar. To make progress in the comparison, we make the following assumption: a certain mode (say $St = 0.3$, $\mu = 0$ inner mode) has the same amplitude at the nozzle exit irrespective of the offset. This is motivated by the broad (and essentially flat) spectrum of disturbances expected in the thin boundary layer at the nozzle exit, that may be deemed to remain unaffected by the nozzle offset. Thus, in the following, every composite eigenfunction is scaled to have a maximum amplitude of unity at the axial station nearest to the nozzle exit ($x = 1$ in our calculations). This is especially important for subsequent quantitative comparisons of the propagated far acoustic field.

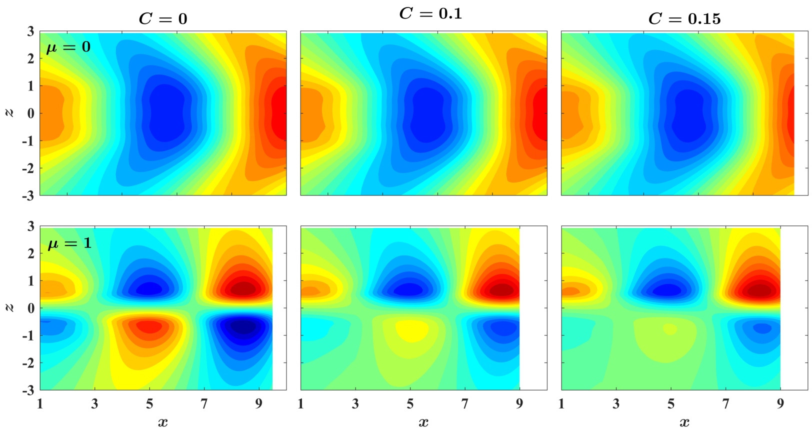

(a)

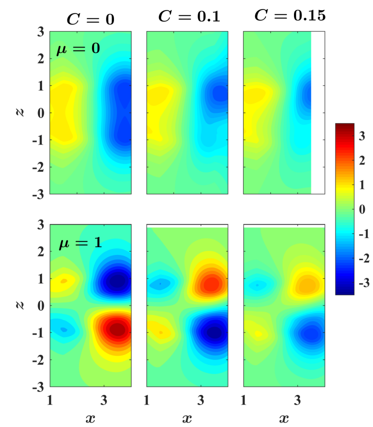

(b)

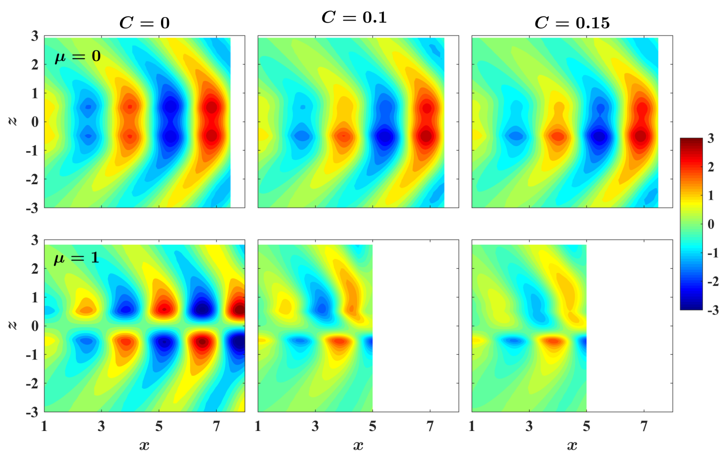

(c)

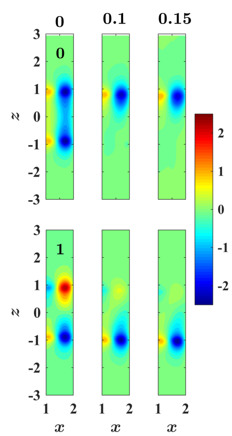

(d)

Figure 4: Real part of composite pressure eigenfunctions for (a, b) $St = 0.1$ and (c, d) $St = 0.3$, in both (a, c) inner and (b, d) outer modes. In each case, results are presented column-wise with various offsets C between the two streams of the jet, and row-wise for the first two μ modes.

Figure 4 presents the composite eigenfunctions for three representative offset values: $C = 0$, 0.1 and 0.15. The quasi-axisymmetric $\mu = 0$ inner mode at $St = 0.1$ does not display any effect of the offset. At $St = 0.3$, this mode appears to be weakened a bit in the top sector ($z > 0$) as the offset increases. Considering now the $\mu = 1$ inner mode, both $St = 0.1$ and 0.3 results display significant weakening in the bottom sector with increasing offset. These changes in the wave packets will be linked to the preferential mitigation of the bottom sector noise in offset jets.

The above trends are reversed in case of the outer modes at both $St = 0.1$ and 0.3. The $\mu = 0$ outer mode displays significant weakening in the bottom sector with increasing offset. Its $\mu = 1$ counterpart, on the other hand, weakens in the top sector. These modes are of course unstable for very short axial spans and also have subsonic phase speed, making them less relevant for the acoustic far field.

Now we propagate the above composite wave packets of the inner modes to the far field using the Kirchhoff surface method. The solution (normalized to unity at the near-nozzle station, as described above) is extracted on the Kirchhoff cylinder of radius $r_{KS} = 3D_p$, and the window described in eqn. (7) is applied prior to Fourier transform in x. Given that the amplitudes of the wave packets are arbitrary (but consistent), the sound pressure level cannot be predicted. Instead, we simply convert the power spectral density (PSD) predicted at various observer locations to decibels using $10\log_{10}(\cdot)$. Thus, the predicted differences in acoustic levels between various offset cases can be read off in dB. Appendix B provides a limited investigation of the robustness of the implementation with respect to the parameters of the method.

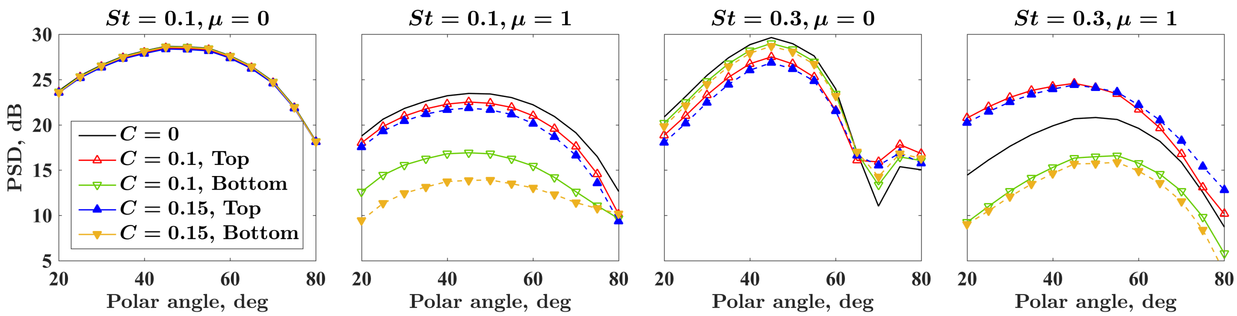

Figure 5: PSD of inner modes on a polar arc of radius $50D_p$.

Figure 5 presents the PSD values on a polar arc of radius $R = 50D_p$ for the inner modes. In general, the polar directivity plots resemble those obtained in experiments on supersonic jets[16], with peak polar angle of about 50°. For the offset jets, a distinction is made between the sound predicted at the top and bottom (dead centres).

No change is discernible in the far field in the case of the $St = 0.1$ and $\mu = 0$ mode. On the other hand, for the $St = 0.1$ and $\mu = 1$ mode, the coaxial jet displays the highest sound level, with some quietening at the top sector with increasing offset, and further quietening at the bottom sector. In case of the $St = 0.3$, $\mu = 0$ mode, the coaxial jet is again the loudest. However, in this case the noise reduction in the bottom sector is less than in the top sector. Finally, in the $St = 0.3$, $\mu = 1$ case, the bottom sector becomes quieter with offset, attended by an increase of loudness in the top sector. All these results are in agreement with the relative amplitudes of the composite eigenfunctions presented in fig. 4.

It is interesting to note that in none of the cases investigated was the bottom sector rendered louder by the offset – it was either made quieter or at worst left unchanged. Thus, our model is able to qualitatively replicate the preferential noise mitigation trends observed in offset dual-stream jets.

V. Conclusion

Offset dual-stream jets have been proposed recently to preferentially quieten the ground sector of jet engines. We present a linear quasi-parallel bi-global stability analysis for such a complex jet configuration with a view to model its noise sources. In the near field, the instability wave packets that simulate such sources indeed display preferential weakening in the bottom sector.

A Kirchhoff surface approach is employed to propagate the near-field pressure to the acoustic far field; this is justified as the primary jet considered for the study is convectively supersonic (Mach 1.5). Very encouraging qualitative agreement is obtained against published experimental results in terms of the trends of selective noise mitigation. Specifically, for every instability mode studied, the bottom sector of the offset jet was either quieter, or no louder, than the coaxial jet counterpart.

Although the scope of this study was limited, the results show promise for understanding and designing quieter non-axisymmetric jets.

APPENDIX

A. Parameters of the bi-global linear stability analysis

The bi-global linear stability calculations have several parameters, and convergence was ensured over all these. Table 1 lists the most important ones. Here, r^f is the radial coordinate where the far-field boundary condition was applied, N_r is the number of points in the radial grid clustered on the lip-line, and N and S are the Fourier azimuthal complexities of the mean flow field and the eigenfunction solved for.

The inner modes for $\mu = 0$ were found to have substantial oscillations far from the centreline, and thus required large radial domains. The number of radial grid points was increased in these calculations to ensure adequate resolution. The azimuthal complexity of the mean flow field is more pronounced for higher offsets. Moreover, better resolution of the azimuthal variation was necessary at the higher frequency.

Modes			r^f	N_r	N			S		
					$C=0$	$C=0.1$	$C=0.15$	$C=0$	$C=0.1$	$C=0.15$
Inner	$St=0.1$	$\mu=0$	20	2500	0	5	7	0	9	11
		$\mu=1$	7	1000	0	10	12	0	14	16
	$St=0.3$	$\mu=0$	20	2500	0	10	12	0	14	16
		$\mu=1$	20	2500	0	10	12	0	14	16
Outer	$St=0.1$	$\mu=0$	15	2000	0	5	7	0	9	11
		$\mu=1$	15	2000	0	5	7	0	9	11
	$St=0.3$	$\mu=0$	15	2000	0	10	12	0	14	16
		$\mu=1$	15	2000	0	10	12	0	14	16

Table 1: Parameters of the stability calculations.

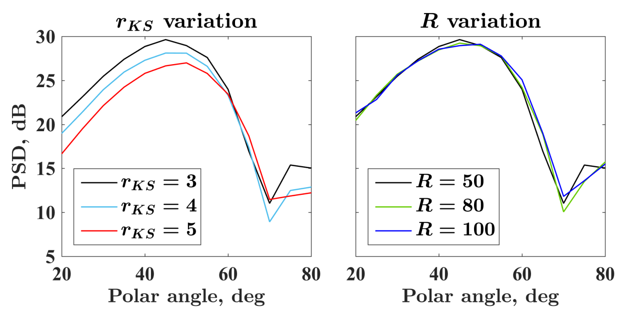

Figure 6: Effect of parameter variation on PSD predicted for the $St = 0.3$, $\mu = 0$ inner mode.

The azimuthal complexity of the mean flow and eigenfunction are high near the nozzle. Thus, these parameters could have been relaxed gradually as the calculations proceeded downstream. This was not pursued.

B. Parameters of the Kirchhoff surface propagation

Since the axial extent of the Kirchhoff surface used in this work is very limited, we study the effect of variation of two of the important parameters of the method. The radius r_{KS} of the Kirchhoff surface is crucial, as it must enclose all the noise sources, and yet be in the well-resolved region of the computation domain. We observe in fig. 6 that the PSD levels decrease with increasing radius r_{KS}, thereby demonstrating a lack of convergence. This is explained by the lack of ‘end-caps’ in the Kirchhoff surface technique, so that sound emanating from the downstream end of the cylinder is not accounted for. As the radius of the Kirchhoff cylinder increases, more and more of the downstream-radiated sound is missed by the calculation. In the results presented earlier, we kept $r_{KS} = 3$ to reduce the severity of this issue.

Figure 6 also shows the effect of the choice of the polar radius of the observer stations, R. The various results are normalized to the common $50D_p$ radius. The calculations are evidently converged with respect to this parameter.

References

[1] M. J. Lighthill. On sound generated aerodynamically. I. General theory. *Proc. R. Soc. Lond. A*, 211(1107):564–587, 1952.

[2] D. Papamoschou. New method for jet noise reduction in turbofan engines. *AIAA Journal*, 42(11):2245–2253, 2004.

[3] D. Papamoschou. Modelling of noise reduction in complex multistream jets. *Journal of Fluid Mechanics*, 834:555–599, 2018.

[4] E. Murakami and D. Papamoschou. Mean flow development in dual-stream compressible jets. *AIAA Journal*, 40(6):1131–1137, 2002.

[5] D. Papamoschou. Fan flow deflection in simulated turbofan exhaust. *AIAA Journal*, 44(12):3088–3097, 2006.

[6] A. Michalke. On the inviscid instability of the hyperbolic-tangent velocity profile. *Journal of Fluid Mechanics*, 19(4): 543–556, 1964.

[7] C. K. W. Tam and D. E. Burton. Sound generated by instability waves of supersonic flows. Part 2. Axisymmetric jets. *Journal of Fluid Mechanics*, 138:273–295, 1984.

[8] P. Jordan and T. Colonius. Wave packets and turbulent jet noise. *Annual Review of Fluid Mechanics*, 45:173–195, 2013.

[9] N. Sohoni and A. Sinha. Modelling noise sources in offset two-stream jets using linear stability theory. In *2018 AIAA/CEAS Aeroacoustics Conference, AIAA Paper 3941*, 2018.

[10] A. Towne, O. T. Schmidt, and T. Colonius. Spectral proper orthogonal decomposition andits relationship to dynamic mode decompositionand resolvent analysis. *Journal of Fluid Mechanics*, 847:821–867, 2018.

[11] A. V. G. Cavalieri, P. Jordan, and L. Lesshafft. Wave-packet models for jet dynamics and sound radiation. *Applied Mechanics Reviews*, 71(2):020802, 2019.

[12] K. Mohseni and T. Colonius. Numerical treatment of polar coordinate singularities. *Journal of Computational Physics*, 157:787–795, 2000.

[13] K. W. Thompson. Time dependent boundary conditions for hyperbolic systems. *Journal of Computational Physics*, 68: 1–24, 1987.

[14] R. B. Lehoucq, D. C. Sorensen, and C. Yang. *ARPACK users' guide: solution of large-scale eigenvalue problems with implicitly restarted Arnoldi methods*. SIAM, 1998.

[15] T. Suzuki and T. Colonius. Instability waves in a subsonic round jet detected using a near-field phased microphone array. *Journal of Fluid Mechanics*, 565:197–226, 2006.

[16] A. Sinha, D. Rodríguez, G. Brès, and T. Colonius. Wavepacket models for supersonic jet noise. *Journal of Fluid Mechanics*, 742:71–95, 2014.

[17] Y. B. Baqui, A. Agarwal, A. V. G. Cavalieri, and S. Sinayoko. A coherence-matched linear source mechanism for subsonic jet noise. *Journal of Fluid Mechanics*, 776:235–267, 2015.

[18] G. Tissot, M. Zhang, F. C. Lajús, A. V. G. Cavalieri, and P. Jordan. Sensitivity of wavepackets in jets to nonlinear effects: the role of the critical layer. *Journal of Fluid Mechanics*, 811:95–137, 2017.

[19] J. B. Freund. Noise sources in a low-Reynolds-number turbulent jet at Mach 0.9. *Journal of Fluid Mechanics*, 438(1): 277–305, 2001.

[20] T. R. Troutt and D. K. McLaughlin. Experiments on the flow and acoustic properties of a moderate-Reynolds-number supersonic jet. *Journal of Fluid Mechanics*, 116:123–156, 1982.

[21] M. D. Dahl and P. J. Morris. Noise from supersonic coaxial jets. Part 2: Normal velocity profile. *Journal of Sound and Vibration*, 200(5):665–699, 1997.

[22] D. Perrault-Joncas and S. A. Maslowe. Linear stability of a compressible coaxial jet with continuous velocity and temperature profiles. *Physics of Fluids*, 20:074102, 2008.

[23] M. Gloor, D. Obrist, and L. Kleiser. Linear stability and acoustic characteristics of compressible, viscous, subsonic coaxial jet flow. *Physics of Fluids*, 25:084102, 2013.

[24] G. Balestra, M. Gloor, and L. Kleiser. Absolute and convective instabilities of heated coaxial jet flow. *Physics of Fluids*, 27 (5):054101, 2015.

[25] A. V. G. Cavalieri, P. Jordan, T. Colonius, and Y. Gervais. Axisymmetric superdirectivity in subsonic jets. *Journal of Fluid Mechanics*, 704:388–420, 2012.